12

Ion beam machine for correction and aspherization of the surface shape of optical elements UIP-300

© A.E. Pestov, M.S. Mikhailenko, A.K. Chernyshev, N.I. Chkhalo, I.G. Zabrodin, A.I. Nikolaev, I.A. Kas'kov, E.S. Antyushin

Institute for physics of microstructure RAS,
603087 Nizhny Novgorod, Russia
e-mail: aepestov@ipm.sci-nnov.ru

Received May 26, 2025
Revised May 26, 2025
Accepted May 26, 2025

An ion-beam machine for correction and aspherization of the surface shape of optical elements for industrial applications (UIP-300) is described. The machine is equipped with three accelerated ion sources (two with focusing ion beam and one with high-current wide-aperture quasi-parallel ion beam) and a goniometer with five degrees of freedom. The realized concept of the movable workpiece made it possible to combine all the methods of ion beam surface treatment (polishing, aspherization, correction and preoperative cleaning) in single machine, as well as to carry out the indicated operations sequentially (without vacuuming the chamber). Accelerated ion sources have been tested, the size of the ion beam and the distribution of the ion current along the aperture of the sources have been determined. It is shown that the available beam sizes from 2.1 to 25 mm and ion currents from 0.3 to 40 mA make it possible to correct the shape of surfaces of any shape and size with both small and significant material removal, and lateral inhomogeneities from tens of millimeters to hundredths of a micron (spatial frequency range up to $9.5 \cdot 10^{-4}\,\mu\mathrm{m}^{-1}$).

Keywords: ion source, ion-beam etching, ion-beam shape correction, roughness.

DOI: 10.61011/TP.2025.09.61856.82-25

Introduction

An ion source (IS) is an electron-vacuum device designed for producing spatially formed fluxes of ions, whose directional velocity is much bigger than a thermal velocity. The modern ion sources can be found in many scientific laboratories and factories. The sources of accelerated ions can be used in various technical processes, in particular, those related to production of micro- and nano-structures (for example, sputtering of films, precise doping of semiconductor crystals to create $p-n$-junctions, ion etching as micro- and nano-treatment of a surface, etc.) [1,2]. During ion-beam etching of the surface, surface layers of materials are removed by physical dissipation with positive ions of inert gases that do not chemically react with the treated material. Usually, for ion purification of a material surface (removal of adsorbed particles) ions with the energy within the range from 20 to 200 eV are used, while for ion etching (removal of layers of a basic material) the ions with the energy from 100 to 10 000 eV are used. With the higher energies, the ions penetrate deeper under the surface into a sample bulk, thereby resulting in reduction of a value of dissipation coefficient and implantation processes prevail. This fact results in using the ion energy of up to 1.5 keV for solving application tasks that are related to surface engineering. This limitation is optimal in terms of minimization of subsurface damage and etching efficiency. Therefore, ion etching has been and is actively applied for shaping optical elements since the end of the 80s, early 90s of the last century [3–5].

Nevertheless, modern development of application optics is actively going towards harnessing a short-wave range of the wavelengths: from the vacuum ultraviolet radiation (VUV, the wavelengths are 100–200 nm) to the extreme ultraviolet radiation (EUV, the wavelengths are 10–100 nm). A scope of the tasks in this range is quite large and extends from scientific ones for exploring physics of the Sun and the upper layers of the atmosphere [6] to applied ones, such as systems for VUV monitoring near-Earth space [7] or systems of advanced EUV lithography [8]. As a unique method of nanodiagnostics, great potential belongs to microscopy in a long-wavelength portion of the soft X-ray range (SXR, the wavelengths are 3–10 nm) [9,10]. Smallness of the wavelength of radiation of the SX and EUV ranges imposes high requirements on a quality of the optical surfaces. Accuracy of the form to achieve spatial resolution that is determined by a Rayleigh diffraction limit [11], according to the Marechal criterion [12], by the standard deviation shall be at least $\lambda/14$ (RMS $< \lambda/14$), where λ is an operating wavelength of the optical system. In order to provide high reflectances of multi-layer mirrors, it is also necessary to provide effective roughness within the spatial frequency range (10^{-3}–$10^{3}\,\mu\mathrm{m}^{-1}$) better than 0.3 nm [13]. These requirements by 1–2 orders exceed requirements to traditional optical elements.

Besides, quite low reflectances of the mirrors of the SX and EUV wavelength ranges require minimization of

a number of elements in an optical circuit. Therefore, in order to solve a number of the tasks, such as, for example, to expand a vision field, aspherization of the optical surface shape is applied. Application of „deep“ and high-accuracy aspherics, including a non-axisymmetric one allow in several times reducing the number of the elements in the optical circuit and producing optical instruments with unique characteristics.

Therefore, it is extremely relevant to develop new methods of treatment of the optical surfaces, which combine high accuracy of material removal, positive effect on roughness, high performance and low cost of a technological process. As of today, the main method that meets all the above-listed requirements is ion-beam treatment.

The literature discusses various diagrams of treatment of the optical parts and proposes alternative to the existing ones [14–17]. In particular, the study [14] proposed to correct the surface shape by a wide-aperture parallel ion beam through masks that are tightly applied to the part surface, with subsequent expansion of open areas. It is obvious that this approach is not optimal, as it results in emergence of steps on the mask edge and, consequently, development of roughness within the medium spatial frequency range. Presently, the mask methods are not applied and maskless correction is used by scanning along the surface with a miniature ion beam [17–21]. The studies [16,17] compare a three-axis diagram (the beam is incident to the surface parallel to the optical axis) and a five-axis diagram (a local normal of the ion beam to the sample surface is maintained). It is shown that both the methods allow achieving nanometer accuracy of the surface shape. But in case of the three-axis diagram mathematical processing is significantly complicated when calculating a scanning map due to projection of the beam to a curvilinear surface and an substantial dependence of an etching rate on the local incident angle. Besides, oblique incidence can result in development of surface roughness [22–24]. Correspondingly, an optimal correction diagram is the five-axis diagram, since it can cope with the above-described problems.

The following diagram is used in almost all the modern machines, for example, those described in [25–27] The treated part is placed stationarily, while the ion source with the small-sized ion beam is installed on a movable table designed to provide linear movements along the three coordinates and inclination in two planes. In various modifications, a part of the degrees of freedom can be handed over to the sample table. The ion beam size is changed by a replaceable diaphragm at a source's output aperture [16,25]. The main disadvantages of this approach include reduction of performance of the process and contamination of the surface of the treated part with products of erosion of the diaphragm edge. Besides, this approach limits a machine functionality by solving the task of correction of local shape errors, which includes scanning along the surface by the small-sized ion beam according to a pre-defined algorithm. In this case, the small-sized low-current beam is required to provide reasonable etching times at small (nanometers and subnanometers) depths of material removal.

Vice versa, for ion polishing and, especially, for deep aspherization (deviation of aspheric surfaces from the nearest sphere can be up to several micrometers and tens of micrometers [7,10]), large and high-current beams of accelerated ions are required.

The present study includes proposition of implementation of another concept of the ion-beam etching machine developed from that described in [28], which combines functions of polishing and aspherization by the wide-aperture high-current ion beam and correction of local shape errors by the small-sized focused ion beam as well as investigation of meshed sources of accelerated ions KLAN-12M, KLAN-53M and KLAN-163M.

1. Description of the machine

A model of the proposed machine for ion-beam treatment of the optical substrates and a diagram of the five-coordinate table for the treated parts are shown in Fig. 1.

The machine includes a vacuum chamber (Fig. 1, *a*), three sources of accelerated ions and a sample table with the five degrees of freedom (Fig. 1, *b*). The additional sixth degree of freedom is provided with a rotatable flap designed to overlap the ion beam and simultaneously to measure an ion current. A depressurization system consists of a prevacuum pump and a turbomolecular pump, which provides a limit residual pressure of $7 \cdot 10^{-5}$ Pa in the operating chamber.

Control of the machine, including vacuum depressurization and pumping of air into the chamber, switching on/off, setting and maintaining operating parameters of the sources of accelerated ions and a position of the sample in relation to the ion beam, sample scanning are fully automated based on the PC-compatible (the processor 80186) controller I-8431 produced by ICP DAS (Taiwan). The controller is connected to an item by periphery modules of the

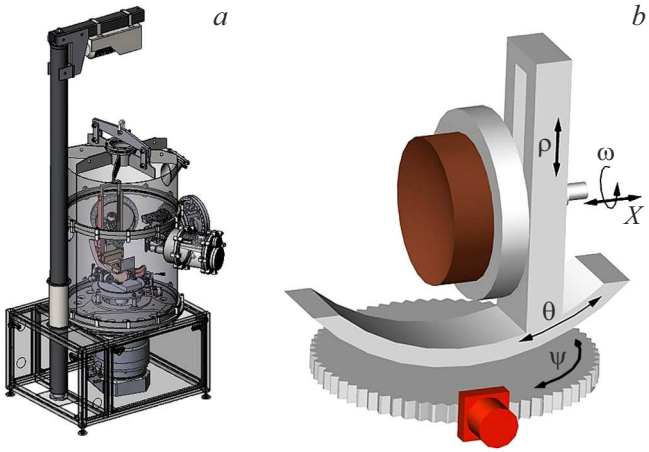

Figure 1. Model of the machine UIP-300 (*a*) and the diagram of the five-coordinate table for the treated parts with indication of possible movements (*b*).

8000 series to be inserted into slots of an expansion unit and modules of the 7000 series inside power units, which are connected to the controller via the RS-485 interface. The controller software is written in the C++ language. The HMI (Human-Machine Interface) is built in the LabView 7.02 environment (National Instruments).

The controller is connected to the HMI-computer via the Ethernet channel at the rate of 10 Mbit/s via the UDP protocol (User Datagram Protocol, the TCP/IP sublevel), which does not require additional equipment of the computer except for the standard LAN-adapter.

1.1. Description of the sample table and the scanning system

A goniometer (Fig. 1, *b*) is equipped with five stepper motors to move the sample and one motor to rotate the flap. Additionally, the sources with focusing of the ion beam are equipped with a linear movement system to bring the source to the treated part for a distance that corresponds to a focal distance of the ion-optical system (IOS). Both the sources are equipped with a rotatable flap also designed to measure the ion current when switching on the source and bringing it to operating parameters. The flap is equipped with a rotating mechanism designed to open it when moving the source from the „parking“ position into the „operating“ position. Purposes and main parameters of the movements are shown in Table 1.

The ion sources are arranged along a circumference of the vacuum chamber with the interval of 60°. Axes of the ion beams of all the sources are in one plane and intersect in a goniometer center (a point of intersection of all the axes of the sample table). The goniometer is rotated around the vertical axis (ψ) to select a direction to the ion source that will be used for a given operation. Due to the three degrees of freedom (ω, X and ρ) any point of an arbitrarily-shaped surface (convex, concave) can be brought to the goniometer center. For this purpose, polar coordinates of the point (ω and ρ) are pre-defined and a deflection arrow (X) is selected by the formula:

$$X = x_0 + R\left(\sqrt{1+\left(\frac{\rho}{R}\right)^2} - \sqrt{1+\left(\frac{D}{2R}\right)^2}\right). \qquad (1)$$

The local normal is set up in this point by inclining the sample:

$$\theta = \arcsin\frac{\rho}{R}. \qquad (2)$$

Here, x_0 — the thickness of the sample; D — the diameter of the sample; R — the sample curvature radius (it is pre-defined taking into account the sign: $R > 0$ — the concave surface; $R < 0$ — the convex surface).

Before a procedure of treatment of the surface with the wide-aperture ion source, the ion source with the closed flap is heated, all the process parameters are set and then the flap (φ) is closed. In order to treat the surface with the small-sized ion beam, the source is brought (L1 or L2) to the surface of the part for the focal distance of the ion-optical system. When the source is moved, accelerating voltage is removed from the meshes (the ion beam is switched off).

Thus, unlike the majority of the machines for ion-beam correction of the surface shape, in which the ion source is placed on a manipulator [25–27], a concept of the movable part is implemented in the present machine. This solution allowed combining in one machine all the methods of ion-beam treatment of the surface, namely, polishing, aspherization and correction. When it is necessary to perform a predefined operation, the substrate is turned towards a required source. Thus, it is possible to significantly increase efficiency of treatment: when significant material removal is necessary, the surface is treated with the high-current wide-aperture ion source; for local correction of errors the source with the small-sized ion beam is used; when significant material removal is necessary (etching for significant depths and/or treating large-size parts), the source with the large size of the ion beam and the high ion current is used; for finishing correction, the ion source with the smaller size of the ion beam and the low ion current is used. Besides, this concept allows performing subsequent treatment by several sources without devacuumization of the system, which is required when solving a number of the tasks, for example, when treating metal optical elements to remove an oxide, when combining procedures of ion-beam polishing and shape correction, etc.

1.2. Ion-beam methods of surface treatment

The methods of treatment of the optical parts, which are available to be realized in the machine, are schematically shown in Fig. 2.

The tasks of aspherization and axisymmetric shape correction are solved by using the wide-aperture high-current ion beam [29–31]. The task means formation of a deterministic dependence of the etching depth (H) on the radius (i.e. $H = H(r)$) on the surface of the treated part.

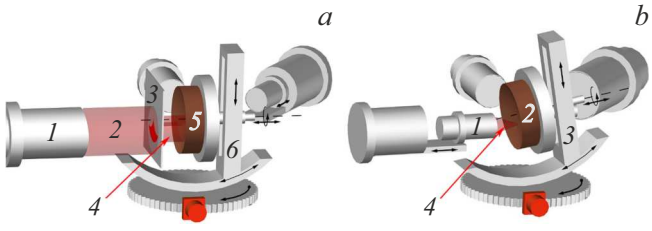

Figure 2. Treatment methods available in the machine UIP-300; *a* — the mode of axisymmetric treatment of the surface: *1* — the wide-aperture ion source (KLAN-163M), *2* — the quasi-parallel ion beam, *3* — the forming diaphragm, *4* — the ion beam downstream of the diaphragm, *5* — the sample, *6* — the goniometer; *b* — the mode of correction of local shape errors: *1* — the source with focusing of the ion beam (KLAN-53M or KLAN-12M), *2* — the sample, *3* — the five-axis goniometer.

Table 1. Purpose and the range of variation of possible movements

Purpose	Variation range	Minimum step
Inclination of the sample, (θ)	$\pm 35^\circ$	0.01°
Rotation around the sample axis, (ω)	$0^\circ - 360^\circ$	0.01°
Linear movement along the sample axis, (X)	0–50 mm	0.02 mm
Linear movement across the sample axis, (ρ)	0–160 mm	0.02 mm
Rotation around the vertical axis, (ψ)	$0^\circ - 120^\circ$	0.01°
Rotation of the flap, (ϕ)	on-off	–
Movement of the focusing source 1, L1	0–200 mm	0.02 mm
Movement of the focusing source 2, L2	0–200 mm	0.02 mm

The method is realized as follows (Fig. 2, *a*). When passing through the diaphragm that forms an ion beam profile *3*, the beam of accelerated ions *2*, which is formed by the wide-aperture ion source *1* with the flat ion-optical system (KLAN-163M), is transformed into a beam of a required section *4* and hits the optical part *5* that is rotated around the central axis and fixed on the rotatable table of the goniometer *6*. Thus, when the part is rotated, a material will be removed from its surface, and it can be described as a certain surface of revolution, which is limited by a generatrix — an etching profile. The etching profile can be pre-defined by an aspherization task or marked from surface shape errors and a center of the etching profile can coincide or not coincide with the part axis; generally, the axis of revolution can be in an arbitrary point of space.

A diaphragm calculation algorithm is reduced to point-wise convolution of a desired etching profile and distribution of the ion current in the beam:

$$\varphi(r) = \frac{\omega}{v(r)} F(r), \tag{3}$$

where $\varphi(r)$ — the mask shape function in the polar coordinates (a column vector of the radii and their respective flare angle; ω — the angular rate of rotation of the part in revolutions per minute (a characteristic of the motorized table); $F(r)$ — the required etching profile as a one-dimensional map, i.e. the dependence of the etching depth on the part radius; $v(r)$ — distribution of the etching rate, which is obtained by normalizing distribution of the ion current in the beam to the etching rate for a given ”gas-target material” pair.

Correction of local shape errors of the optical surfaces in the UIP-300 industrial machine for ion-beam treatment of the optical parts involves reduction of an amplitude of heterogeneities with lateral sizes that exceed 1 mm (Fig. 2, *b*). When implementing the method, the ion source with focusing of the ion beam *1* is used, and during treatment a local normal to the surface (which is provided by the degrees of freedom of the goniometer *3*) is maintained in each point of the part *2*. The part is treated by the small-sized Gaussian-shaped ion beam *4* when it scans along the surface of the part. Depending on the lateral size and a spread of heights of heterogeneities, a source with focusing of the ion beam with a waist area of Ø10 mm (KLAN-53M) or Ø2 mm (KLAN-12M) is selected. Scanning is performed by rotating the part and moving it along the radius for a scanning step after each revolution. Each step includes tuning of the coordinates (X — the distance from the ion source to the part and φ — the angle of inclination of the part) to maintain the local normal to the surface and the pre-defined ”source-sample” distance. In order to perform a shape correction procedure, an etching map is calculated by the software based on an algorithm described in [32]. At the entrance, the software receives the interferometer-measured surface map and spatial distribution of the etching rate, which is selected from an etching crater (a method of recording the etching crater is described with more details in Section 2.2). They were convoluted then and at the exit there is the etching map which is output to be a set of coordinates of the surface points and their respective etching times.

1.3. Ion sources

Three technological sources of accelerated ions are applied in the machine (Fig. 3), whose technical characteristics are shown in Table 2.

As can be seen from Fig. 3, *b, c* and Table 2, the ion-optical systems of the sources KLAN-12M and KLAN 53M are designed as a pair of concave meshes with the curvature radius of $R = 20$ and 70 mm, respectively. Thus, the focal distance (the waist area) that corresponds to a minimum size of the ion beam is at a distance that is close to these values. As said above, when performing the procedure of correction of the local shape errors, scanning is performed with maintaining the pre-defined ”source-sample” distance. It means that during operation the source shall be at the distance of 20 mm (for KLAN-12M) or 70 mm (for KLAN-53M) to the surface of the part. However, when accelerating (setting the operating parameters and heating) of the ions source, the ion beam shall hit the surface of the part. Therefore, a flap shall be between the source of accelerated ions and the part, and it shall open for the time of the ion treatment process and close during adjustment and when the process is complete. Besides, the flap must be electrically coupled to a „ground“ potential via a resistance

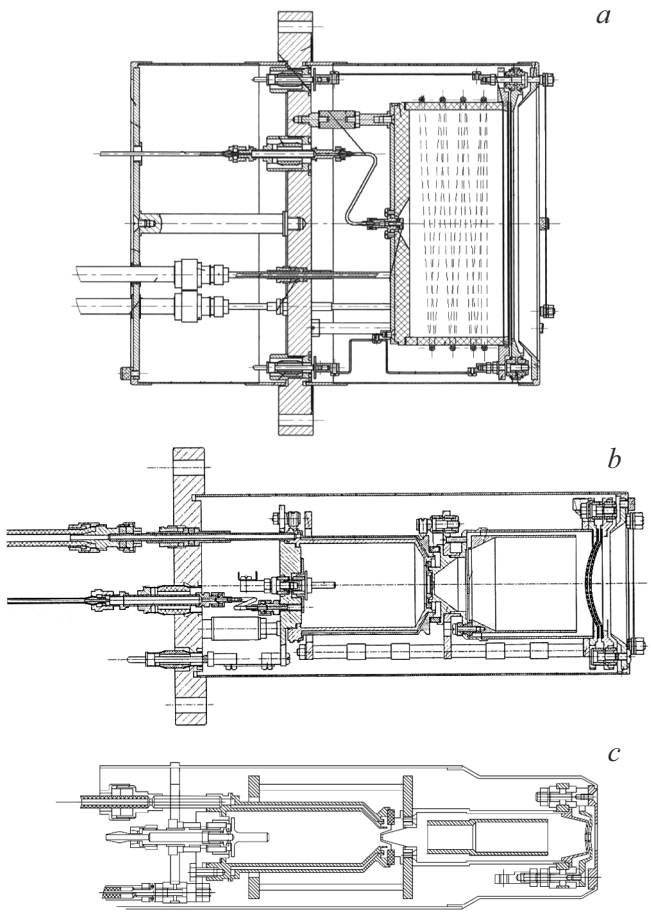

Figure 3. Diagrams of the ions sources for the UIP-300 machine: *a* — the source KLAN-163M — the high-frequency source with the flat IOS; *b* — the source KLAN-53M — the source with a field emission cathode and the focusing IOS; *c* — the source KLAN-12M — the source with the field emission cathode and the focusing IOS.

to enable controlling, by current flow through the resistor, a value of the ion current hitting the flap, in particular, to control neutralization of a positive charge of the ion beam when operating dielectric materials.

Rotatability of the table with the part fixed thereon from one source towards another is provided for the sources KLAN-12M and KLAN-53M in two positions: the parking position, in which the source is in a non-operating state (the distance to the goniometer center is 200 mm), and the operating position, when the source is brought to the goniometer source.

2. Study of the ion sources

Implementation of the methods described in Section 1.2 requires qualification of the characteristics of the sources of accelerated ions (the ion current, distribution of the ion current along the aperture, the focusing spot diameter, the focal distance). These studies were performed according to a diagram shown in Fig. 4.

The goniometer *1* was rotated towards the selected source *2* and its parameters were tested.

2.1. Wide-aperture source (KLAN-163M)

The high-current wide-aperture source of accelerated ions KLAN-163M with the quasi-parallel ion beam is provided with the flat two-meshed IOS geometry. Due to the large output aperture of the beam (Ø160 mm) and the high ion current (up to 200 mA) the source allows performing significant material removals simultaneously from a large area of the part (deep aspherization, axisymmetric correction, ion polishing).

The ion beam of the source KLAN-163M was studied at a distance that corresponds to a distance from a source exit to the goniometer center in the UIP-300 machine (the distance from the output source mesh to the goniometer center is 270 mm), i.e. distribution of the ion current was studied in a plane that is perpendicular to the axis of the ion source and passes through the goniometer center. The value of the ion current is proportional to the etching rate [22], therefore the experiment was as follows. A mask (a photoresist strip of the width of 1 mm) was applied to an experimental sample of the fused-quartz plate of the length of 150 mm and the width of 12 mm (the UV lithograph was used [33]). Then, this experimental sample was placed on the sample table that is arranged at the distance of 270 mm from the output source mesh so as the strip edge passed through the ion beam's axis along its radius (Fig. 5).

During ion etching, a mask boundary had a step formed, whose height was proportional to a density of the ion current in this point. By measuring a dependence of the step height on the coordinate, it is possible to determine a dependence of the etching rate on the radius, which is proportional to the density of the ion current in this point. The so-obtained dependences for various accelerating voltages are shown in Fig. 6.

As it is clear from the figure, the full size of the beam at the half maximum is about 160 mm. And, when using respective shaped diaphragms at the source output, it makes it possible to treat the parts of the diameter of up to 320 mm. It was also found that it was possible to operate the accelerating voltage $U_{acc} = 200$ V, thereby providing performance of a procedure of cleaning the part surface with oxygen ions without dissipation of the part material.

2.2. Small-sized source with the focusing IOS (KLAN-12M)

The parameters of operation of KLAN-12M were studied to investigate a size and a shape of the ion beam in a dependence on the distance to the source aperture exit.

In order to study the ion beam size, an etching crater was formed on the flat fused quartz plate that was pre-

Table 2. Main characteristics of the ion sources

Characteristic	KLAN-163M	KLAN-53M	KLAN-12M
Source type	Radio-frequency $f = 2.0$ MHz	Meshed, with field emission hollow cathode	Meshed, with field emission hollow cathode
Ion-optical system	Two-meshed, flat, the material — molybdenum	Two-meshed, concave, $R = 70$ mm, the material — titanium	Two-meshed, convex, $R = 20$ mm, the material — titanium
Working gas	Inert gases, O_2, N_2, C_2H_8, etc.	Inert gases, N_2	Inert gases, N_2
Operating pressure, Pa	$3 \cdot 10^{-2}$	$3 \cdot 10^{-2}$	$3 \cdot 10^{-3}$
Size of the ion beam, mm	Ø160	Ø10	Ø2
Maximum ion current, mA	200	80	1
Ion energy, eV	300–1500	300–1500	300–1500
Energy spread, eV	±3	±3	±3
Overall dimensions, mm	Ø221 × 165	Ø99.6 × 235	Ø48 × 166

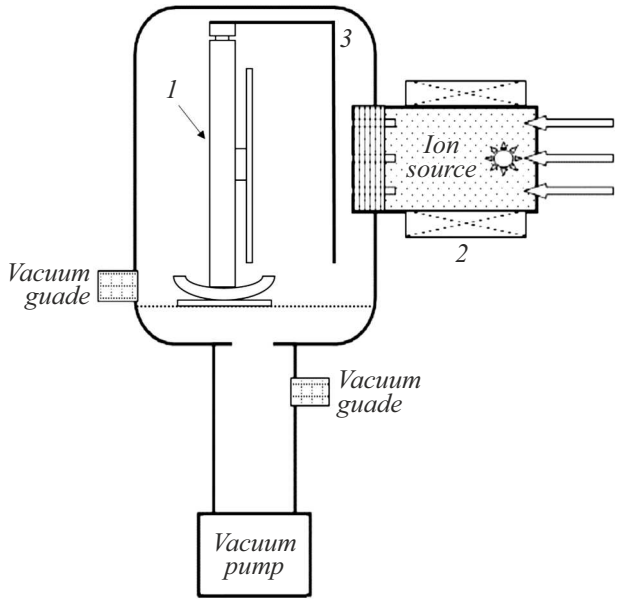

Figure 4. Diagram of the experiment for qualification of the parameters of the sources: *1* — the goniometer with the five degrees of freedom; *2* — the ion source; *3* — the flap.

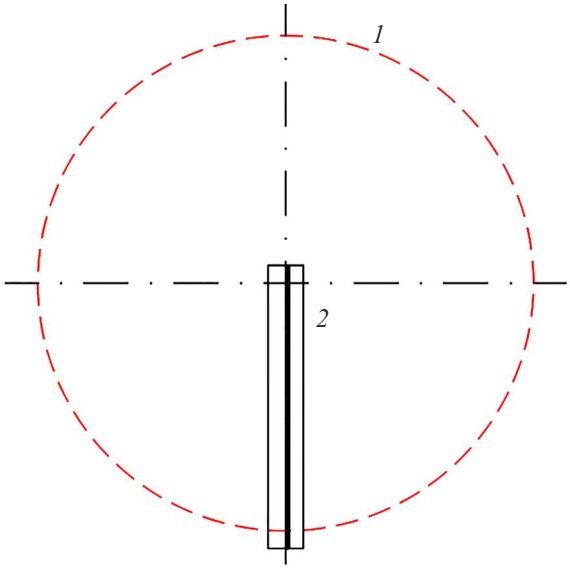

Figure 5. Diagram of the experiment for studying the etching rate along the source aperture: *1* — the ion beam; *2* — the sample.

measured on the laser interferometer Zygo VeriFire 4. For this purpose, the sample was brought to the source for a pre-defined distance, the flap was opened and it was etched with the fixed source and the fixed sample for some time T. By analyzing the produced crater, it is possible to calculate linear sizes of the ion beam and to built spatial distribution of the etching rate. Thus, a series of the experiments was conducted to form craters at various distances to the ion source. The operating ion energy was selected to be $E_{ion} = 1250$ eV, as it was shown in the study [22] that the beams with the ion energy $E_{ion} = 1250$ eV are applied for effective ion-beam treatment of the optical materials.

Fig. 7, *a* shows the measured map of the surface of the fused quartz sample before forming the etching crater on it, while Fig. 7, *b* shows the sample surface map after ion irradiation and the etching crater is clearly seen on.

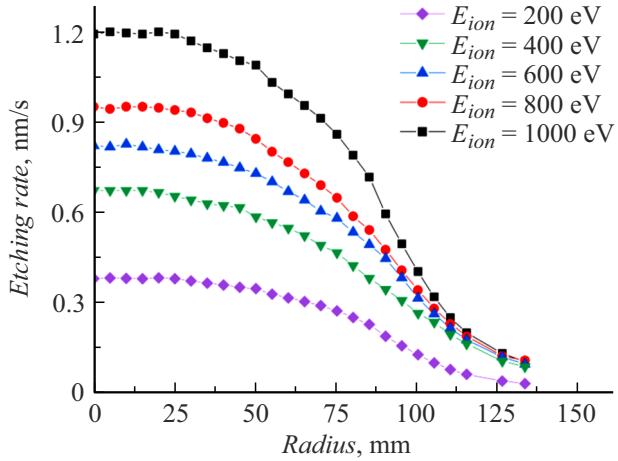

Figure 6. Distribution of the etching rate along the radius of the source KLAN-163M (the distance is 270 mm; the gas is Ar; I_{ion} = 150 mA).

However, the presented map is not informative, as it has a large contribution by the initial shape of the surface. In order to identify the etching crater proper, we have pointwisely compared the surface maps measured before and after the ion irradiation process. A difference of the maps is shown in Fig. 7, *c*. The produced difference maps describes spatial distribution of the material removed from the surface. Fig. 7, *d* shows sections of the difference map along the vertical and the horizontal as well as an approximation of the obtained sections by the Gaussian distribution. As can be seen, the craters are Gaussian-like and can be characterized by means of a width at half maximum

Fig. 8 shows a dependence of the width of the ion beams on the distance between the ion source and the sample, which is plotted by the studies of the craters. At this, the parameters of the ion source were as follows: the ion current was 0.3 mA, the ion energy was 1250 eV, the operating gas pressure in the chamber was $2.2 \cdot 10^{-5}$ Torr and the cathode current was 50 mA.

It can be seen that the minimum size of the ion beam was 2.1 mm, which, according to the study in the paper [34], allows effectively reducing the surface shape errors with the spatial frequencies of up to $9.5 \cdot 10^{-4}\,\mu\text{m}^{-1}$. Besides, it is found that with increase of the distance the lateral size of the crater is increased, which can be used for correcting the shape of the large-sized optical elements with low-frequency shape errors. The large size of the beam will allow passing

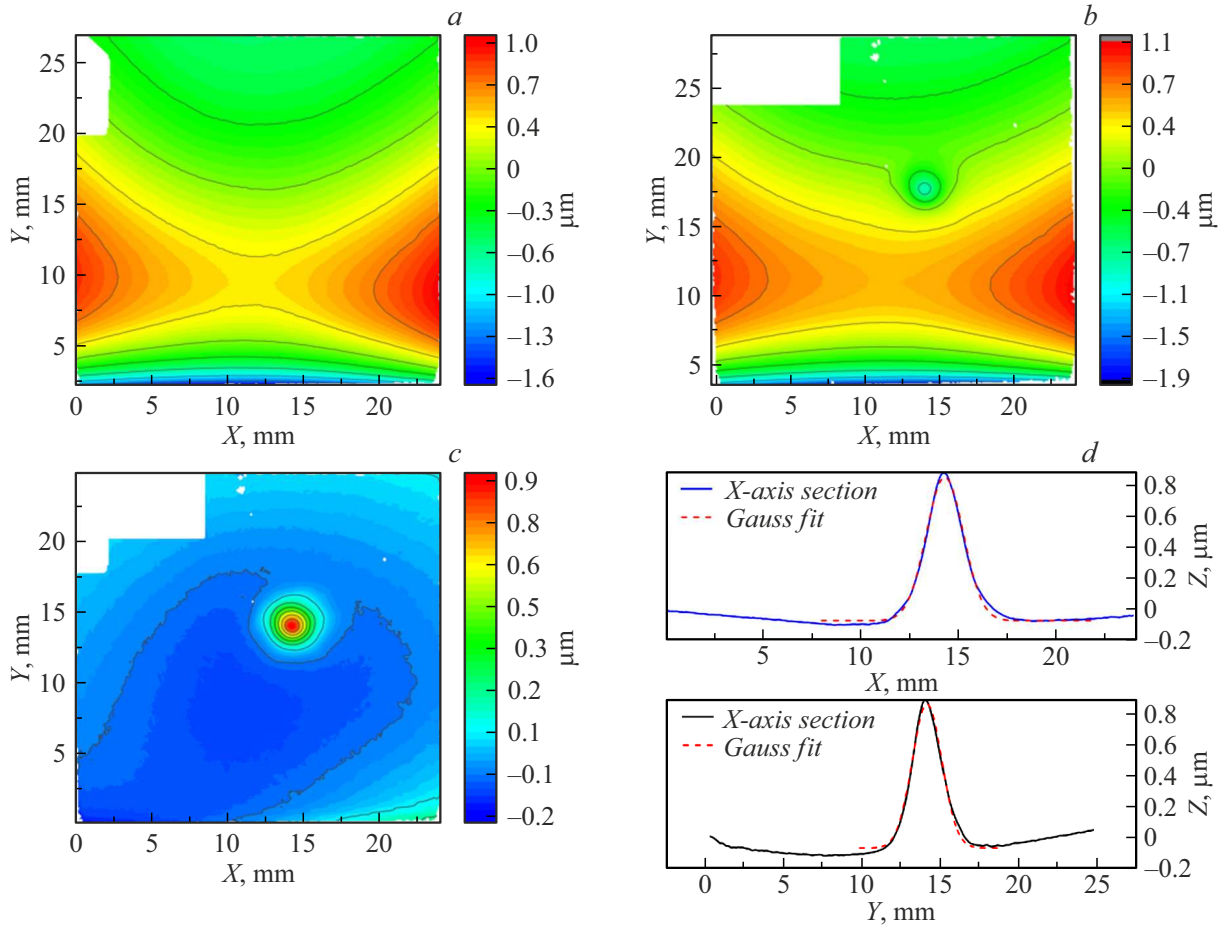

Figure 7. Study of the etching crater: *a* — the initial surface; *b* — the surface with the crater; *c* — the crater; *d* — the crater sections.

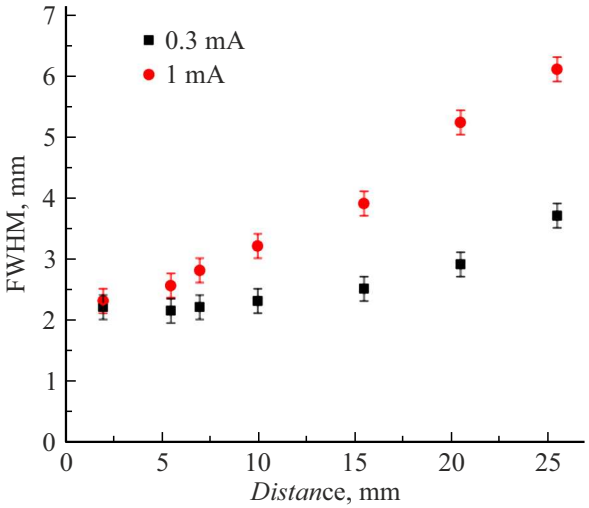

Figure 8. Dependence of the half-width of the etching crater on the „source–sample“ distance. The source is KLAN-12M ($E_{ion} = 1250$ eV, $I_{ion} = 0.3$ and 1 mA).

along the surface with a large step, thereby saving the time for movement and, therefore, the time of the procedure as a whole.

It was found during the study that when the ion source was at a distance of two millimeters to the test sample, the beam was not described by normal distribution (Fig. 9). This change is related to the fact that the distance to the sample was less than the focal distance, which is why the spatial distribution exhibits contribution by separate beam elements. Orientation of separate spots that are visible in the distribution coincides with orientation of cells on a grid of the IOS of the ion source.

Thus, the characteristics of the ions beam of the source KLAN 12M have been studied. In particular, we have obtained the dependences of the ion beam size on the distance to the output aperture and shown viability of application of the source for correction of the local surface shape errors. The ion beam's minimum size of 2.1 mm allows effectively reducing the surface shape errors with the spatial frequencies of up to $9.5 \cdot 10^{-4}\,\mu\text{m}^{-1}$.

2.3. Source with the focusing IOS (KLAN-53M)

The similar studies have been performed for the source KLAN-53M. Results of the experiments for forming the craters at the various distances to the ion source for the ion energy $E_{ion} = 1250$ eV are shown in Fig. 10. As can be seen, there is a series of the craters formed on the sample at the ion current of 20 mA, whose size was analyzed and plotted (Fig. 11).

As can be seen, the minimum size of the ion beam with $E_{ion} = 1250$ and 10 mA was 6.2 mm, which is overlapped with the maximum recorded beam size for the source KLAN-12M. This continuous dependence will allow correcting the shape of the surfaces of any shape and overall dimensions with the lateral sizes of heterogeneities from tens of millimeters to hundredths of micrometers (the spatial frequency range of up to $9.5 \cdot 10^{-4}\,\mu\text{m}^{-1}$).

Conclusion

The study describes the UIP-300 industrial machine for ion-beam treatment of the optical parts. The machine includes the vacuum chamber with the two-step depressurization system, the sample table with the five degrees of freedom (the goniometer) and the three sources of accelerated ions. The goniometer is designed to treat parts of up to Ø300 mm and of the thickness of 50 mm, thereby providing the local normal to the arbitrarily-shaped surface (flat, convex, concave).

The machine is designed from a prototype that is described with details in the paper [28]. Unlike the prototype, in addition to the wide-aperture source of accelerated ions with the quasi-parallel ion beam (KLAN-163M), which allows performing polishing and aspherization of the surface through the diaphragm that forms the ion beam profile, the UIP-300 also includes the sources with focusing of the ion

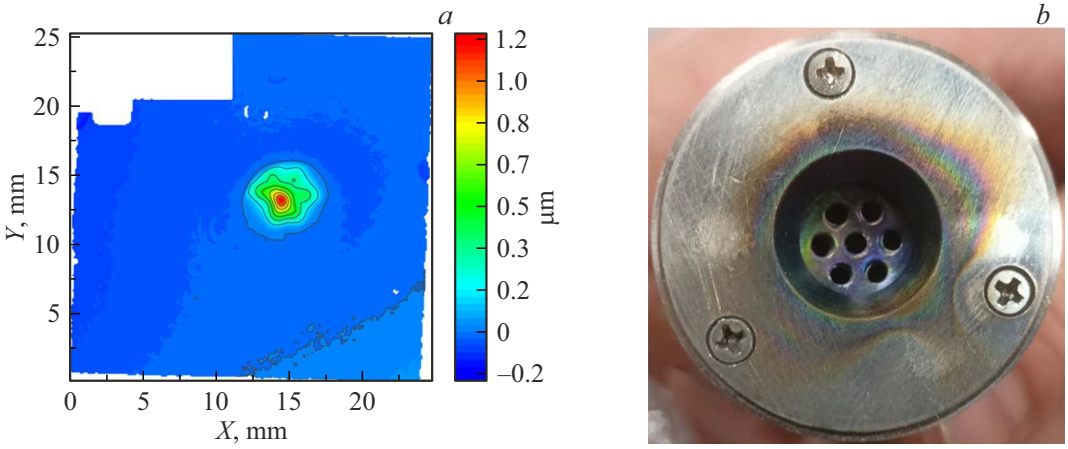

Figure 9. Etching crater at the distance of 2 mm to the source (a) and the photo of the accelerating mesh of the IOS (b).

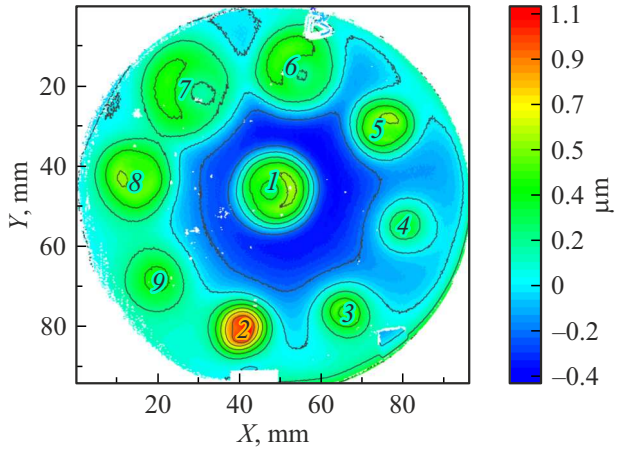

Figure 10. Etching craters for the source KLAN-53M (I_{ion} = 20 mA, 1250 eV).

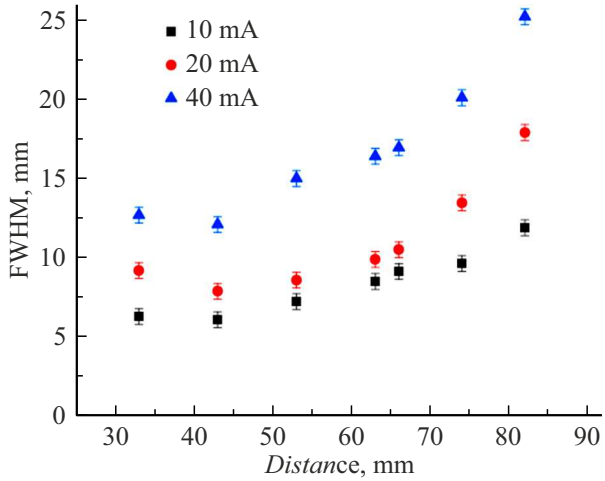

Figure 11. Dependence of the half-width of the etching crater on the „source–sample“ distance. The source is KLAN-53M (E_{ion} = 1250 eV; I_{ion} = 10, 20 and 40 mA).

beam (KLAN-53M and KLAN-12M), which are installed on motorized platforms designed to bring the source to the surface of the treated part for a pre-defined (focal) distance. The sources with focusing of the ion beam are designed for correcting the local shape errors in a maskless method. The specific feature of these sources is absence of a diaphragm that cuts off the ion beam, which allowed significantly improving treatment efficiency by using the full current of the ion beam as well as provided elimination of a pernicious effect of contamination of the surface of the treated part with products of erosion of the diaphragm edge.

The study also included testing the applied sources of accelerated ions. The dependences of the value of the ion current on the radius are recorded for the wide-aperture source KLAN-163M at the various accelerating voltages. The distribution of the ion current along the aperture is necessary for calculating a section of cutting-off diaphragms that are used for the procedures of axisymmetric shape correction, aspherization, ion polishing and preoperational cleaning of the surface. For the sources with focusing of the ion beam (KLAN-53M and KLAN-12M), we have recorded the size and the shape of the etching crater for the various ion currents and the various distance to the output aperture. The crater shape is necessary for calculating the etching map for the procedure of correction of the local shape errors. For the source KLAN-12M the ion beams varies within the range 2.1–6 mm and the ion current is up to 1 mA, while for the source KLAN-53M the ion beam varies within the range 6.2–25 mm and the ion current is up to 40 mA. Thus, application of the two sources with focusing of the ion beam extends the functionality of capabilities of treating the heterogeneities in the height and the lateral sizes. I.e., a continuous range of variation of the ion beam's waist diameter from the minimum one of 2.1 mm to about 25 mm and variation of the ion current from 0.3 to 40 mA allows correcting the shape of the surfaces of any shape and overall dimensions with both small and significant material removal and the lateral sizes of heterogeneities from tens of millimeters to hundredths of micrometers (the spatial frequency range of up to $9.5 \cdot 10^{-4}\,\mu\text{m}^{-1}$).

Funding

The study was carried out with support by grant from the Russian Science Foundation 21-72-30029-P in terms of developing methods and investigation of parameters of the ion beams and under the state assignment FFUF-2024-0022 in terms of upgrading of process equipment. Facilities of Center „Physics and technology of micro- and nanostructures“ at IPM RAS were used.

Conflict of interest

The authors declare that they have no conflict of interest.

References

[1] J.R. Conrad, J.L. Radtke, R.A. Dodd, F.J. Worzala, N.C. Tran. J. Appl. Phys., **62** (11), 4591 (1987). DOI: 10.1063/1.339055
[2] G. Dearnaley, K. Kandiah, R.S. Nelson. Phys. Bull., **20**, 165 (1969). DOI: 10.1088/0031-9112/20/5/002
[3] L.N. Allen, H.W. Romig. Proc. SPIE, **1333**, 22 (1990). DOI: 10.1117/12.22786
[4] S.R. Wilson, D.W. Reicher, J.R. McNeil. Proc. SPIE, **966**, 74 (1988). DOI: 10.1117/12.948051
[5] N.P. Eisenberg, R. Carouby, J. Broder. Proc. SPIE, **1038**, 279 (1988). DOI: 10.1117/12.951062
[6] C. Hoffman, T.G. Giallorenzi, L.B. Slater. Appl. Opt., **54** (31), F268 (2015). DOI: 10.1364/AO.54.00F268
[7] A.K. Akopov, M.N. Brychikhin, Yu.A. Plastinin, A.A. Rizvanov, I.L. Strulya, Ya.O. Eikhorn, I.V. Malyshev, A.E. Pestov, V.N. Polkovnikov, M.N. Toropov, N.I. Chkhalo. Kosmonavtika i raketostroenie, **4** (78), 77 (2014) (in Russian).
[8] Ch. Wagner, N. Harned. Nat. Photonics, **4**, 24 (2010). DOI: 10.1038/nphoton.2009.251

[9] Y. Platonov, J. Rodriguez, M. Kriese, E. Gullikson, T. Harada, T. Watanabe, H. Kinoshita. Proc. SPIE, **8076**, 80760N-2 (2011). DOI: 10.1117/12.889519
[10] M.M. Barysheva, A.E. Pestov, N.N. Salashchenko, M.N. Toropov, N.I. Chkhalo. Phys.-Usp., **55** (7), 681 (2012). DOI: 10.3367/UFNe.0182.201207c.0727
[11] M. Born, E. Wolf. *Resolving power of image-forming system*. In *Principles of Optics* (Cambridge University, 1999), Sec. 8.6.2, p. 461.
[12] M. Born, E. Wolf. *Tolerance conditions for primary aberrations*. In *Principles of Optics* (Cambridge University, 1999), Sec. 9.3, p. 528.
[13] K. Murakami, T. Oshino, H. Kondo, H. Chiba, H. Komatsuda, K. Nomura, H. Iwata. Proc. SPIE, **6921**, 69210Q (2008). DOI: 10.1117/12.772435
[14] N.I. Chkhalo, E.B. Kluenkov, A.E. Pestov, V.N. Polkovnikov, D.G. Raskin, N.N. Salashchenko, L.A. Suslov, M.N. Toropov. Nucl. Instrum. Methods Phys. Res. A, **603** (1-2), 62 (2009). DOI: 10.1016/j.nima.2008.12.160
[15] M. Idir, L. Huang, N. Bouet, K. Kaznatcheev, M. Vescovi, K. Lauer, R. Conley, K. Rennie, J. Kahn, R. Nethery, L. Zhou. Rev. Sci. Instrum., **86** (10), 016120 (2015). DOI: 10.1063/1.4934806
[16] W. Liao, Y. Dai, X. Xie, L. Zhou. Appl. Opt., **53** (19), 4266 (2014). DOI: 10.1364/AO.53.004266
[17] W. Liao, Y. Dai, X. Xie, L. Zhou. Appl. Opt., **53** (19), 4275 (2014). DOI: 10.1364/AO.53.004275
[18] M. Xu, Y. Dai, X. Xie, L. Zhou, W. Liao. Appl. Opt., **54** (27), 8055 (2015). DOI: 10.1364/AO.54.008055
[19] A. Schindler. *Tutorial on Recent Advances in Ion Beam and Plasma Jet Processing* (Optical Fabrication and Testing 2012, Monterey, California United States 24–28 June 2012), p. OW4D.1.
[20] O. Schmelzer, R. Feldkamp. Proc. SPIE, **9633**, 96330E (2015). DOI: 10.1117/12.2196871
[21] Th. Arnold, G. Boehm, H. Paetzelt, F. Pietag. Proc. SPIE, **9442**, 944204 (2015). DOI: 10.1117/12.2175491
[22] N.I. Chkhalo, S.A. Churin, M.S. Mikhaylenko, A.E. Pestov, V.N. Polkovnikov, N.N. Salashchenko, M.V. Zorina. Appl. Opt., **55** (6), 1249 (2016). DOI: 10.1364/AO.55.001249
[23] W. Liao, Y. Dai, X. Xie, L. Zhou. Appl. Opt., **52** (16), 3719 (2013). DOI: 10.1364/AO.52.003719
[24] A. Keller, S. Facsko, W. Moller. J. Phys., **21**, 495305 (2009). DOI: 10.1088/0953-8984/21/49/495305
[25] Electronic source. Available at: http://www.opteg.com
[26] Electronic source. Available at: http://www.meyerburger.com/
[27] Electronic source. Available at: http://www.ntg.de/
[28] N.I. Chkhalo, I.A. Kaskov, I.V. Malyshev, M.S. Mikhaylenko, A.E. Pestov, V.N. Polkovnikov, N.N. Salashchenko, M.N. Toropov, I.G. Zabrodin. Prec. Eng., **48**, 338 (2017). DOI: 10.1016/j.precisioneng.2017.01.004
[29] A.M. Karger. Appl. Opt., **12** (3), 451 (1973). DOI: 10.1364/AO.12.000451
[30] L.A. Cherezova, A.V. Mikhaĭlov, A.P. Zhevlakov. J. Opt. Technol., **73** (11), 812 (2006). DOI: 10.1364/JOT.73.000812
[31] M.V. Zorina, I.M. Nefedov, A.E. Pestov, N.N. Salashchenko, S.A. Churin, N.I. Chkhalo, J. Surf. Invest., **9**, 765 (2015). DOI: 10.7868/S0207352815080193
[32] M.S. Mikhailenko, A. Chernyshev, N. Chkhalo, I. Malyshev, A. Pestov, R. Pleshkov, R. Smertin, M. Svechnikov, M. Toropov. Prec. Eng., **69**, 29 (2021). DOI: 10.1016/j.precisioneng.2021.01.006
[33] A.I. Artyukhov, S.S. Morozov, D.V. Petrova, N.I. Chkhalo, R.A. Shaposhnikov. ZhTF, **94** (8), 1295 (2024) (in Russian). DOI: 10.61011/JTF.2024.08.58557.165-24
[34] M.S. Mikhailenko, A.E. Pestov, N.I. Chkhalo, L.A. Goncharov, A.K. Chernyshev, I.G. Zabrodin, I. Kaskov, P.V. Krainov, D.I. Astakhov, V.V. Medvedev. Nucl. Instrum. Methods Phys. Res. A, **1010**, 165554 (2021). DOI: 10.1016/j.nima.2021.165554

Translated by M.Shevelev